Article

Cancer Cell

Mutations in the SIX1/2 Pathway and the DROSHA/DGCR8 miRNA Microprocessor Complex Underlie High-Risk Blastemal Type Wilms Tumors

Graphical Abstract

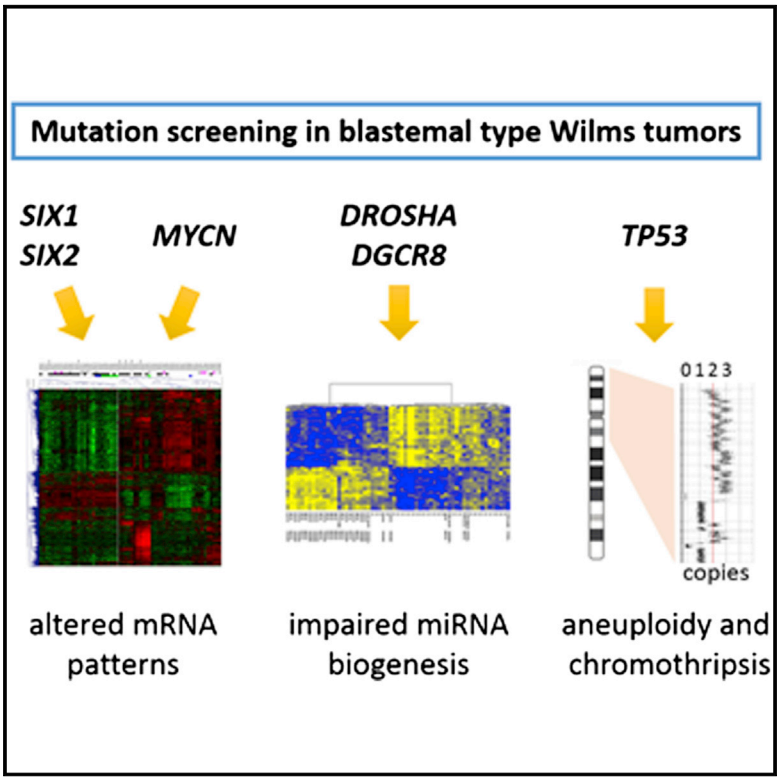

Authors

Jenny Wegert, Naveed Ishaque, ..., Marcel Kool, Manfred Gessler

Correspondence

gessler@biozentrum.uni-wuerzburg.de

In Brief

Blastemal type Wilms tumors are associated with poor prognosis. Wegert et al. identify recurrent mutations in *SIX1* and *SIX2* that correlate with high proliferation and in *DROSHA* and *DGCR8* that affect miRNA biogenesis, as well as a high frequency of *IGF2* overexpression in these tumors.

Highlights

- *SIX1/2* mutations in blastemal type Wilms tumors induce a proliferation signature
- DROSHA/DGCR8 microprocessor mutations lead to a broad decrease in miRNA processing
- *TP53* mutations are associated with aneuploidy, chromothripsis, and high lethality
- *IGF2* and *MYCN/FBXW7* alterations are frequent in blastemal type tumors

Accession Numbers

GSE53224
GSE57370
GSE60081

Wegert et al., 2015, Cancer Cell *27*, 298–311
February 9, 2015
http://dx.doi.org/10.1016/j.ccell.2015.01.002

CellPress

Cancer Cell
Article

Mutations in the SIX1/2 Pathway and the DROSHA/DGCR8 miRNA Microprocessor Complex Underlie High-Risk Blastemal Type Wilms Tumors

Jenny Wegert,[1,18] Naveed Ishaque,[2,3,18] Romina Vardapour,[1] Christina Geörg,[3] Zuguang Gu,[2,3] Matthias Bieg,[2,3] Barbara Ziegler,[1] Sabrina Bausenwein,[1] Nasenien Nourkami,[4] Nicole Ludwig,[5] Andreas Keller,[5] Clemens Grimm,[6] Susanne Kneitz,[7] Richard D. Williams,[8] Tas Chagtai,[8] Kathy Pritchard-Jones,[8] Peter van Sluis,[9] Richard Volckmann,[9] Jan Koster,[9] Rogier Versteeg,[9] Tomas Acha,[10] Maureen J. O'Sullivan,[11] Peter K. Bode,[12] Felix Niggli,[12] Godelieve A. Tytgat,[13] Harm van Tinteren,[13] Marry M. van den Heuvel-Eibrink,[14] Eckart Meese,[5] Christian Vokuhl,[15] Ivo Leuschner,[15] Norbert Graf,[4] Roland Eils,[2,3,16] Stefan M. Pfister,[17] Marcel Kool,[17,19] and Manfred Gessler[1,19,*]

[1]Theodor-Boveri-Institute/Biocenter, Developmental Biochemistry, and Comprehensive Cancer Center Mainfranken, Wuerzburg University, 97074 Wuerzburg, Germany
[2]Division of Theoretical Bioinformatics (B080), German Cancer Research Center (DKFZ), 69121 Heidelberg, Germany
[3]Heidelberg Center for Personalised Oncology (DKFZ-HIPO), German Cancer Research Center (DKFZ), 69121 Heidelberg, Germany
[4]Department of Pediatric Oncology and Hematology, Saarland University Hospital, 66421 Homburg, Germany
[5]Department of Human Genetics, Saarland University, 66421 Homburg, Germany
[6]Theodor-Boveri-Institute/Biocenter, Biochemistry, Wuerzburg University, 97074 Wuerzburg, Germany
[7]Theodor-Boveri-Institute/Biocenter, Physiological Chemistry, Wuerzburg University, 97074 Wuerzburg, Germany
[8]UCL Institute of Child Health, London WC1N 1EH, UK
[9]Department of Oncogenomics, Academic Medical Center, University of Amsterdam, 1007 MB Amsterdam, the Netherlands
[10]Unidad de Oncología Pediátrica, Hospital Materno-Infantil de Málaga, 29011 Malaga, Spain
[11]National Children's Research Centre, Our Lady's Children's Hospital, Crumlin, and Trinity College, Dublin 12, Ireland
[12]Department of Pediatric Hematology and Oncology, Children's University Hospital, 8032 Zurich, Switzerland
[13]Department of Pediatric Oncology, Emma Children's Hospital, Academic Medical Center, University of Amsterdam, 1007 MB Amsterdam, the Netherlands
[14]Department of Pediatric Oncology, Erasmus MC-University Medical Center Rotterdam, 3000 CA Rotterdam, the Netherlands
[15]Kiel Paediatric Cancer Registry, Christian Albrechts University, 24105 Kiel, Germany
[16]Department for Bioinformatics and Functional Genomics, Institute for Pharmacy and Molecular Biotechnology (IPMB) and BioQuant, Heidelberg University, 69121 Heidelberg, Germany
[17]Division of Pediatric Neurooncology, German Cancer Research Center (DKFZ), 69120 Heidelberg, Germany
[18]Co-first author
[19]Co-senior author
*Correspondence: gessler@biozentrum.uni-wuerzburg.de
http://dx.doi.org/10.1016/j.ccell.2015.01.002

SUMMARY

Blastemal histology in chemotherapy-treated pediatric Wilms tumors (nephroblastoma) is associated with adverse prognosis. To uncover the underlying tumor biology and find therapeutic leads for this subgroup, we analyzed 58 blastemal type Wilms tumors by exome and transcriptome sequencing and validated our findings in a large replication cohort. Recurrent mutations included a hotspot mutation (Q177R) in the homeo-domain of *SIX1* and *SIX2* in tumors with high proliferative potential (18.1% of blastemal cases); mutations in the *DROSHA/DGCR8* microprocessor genes (18.2% of blastemal cases); mutations in *DICER1* and *DIS3L2*; and alterations in *IGF2*, *MYCN*, and *TP53*, the latter being strongly associated with dismal outcome. *DROSHA* and *DGCR8* mutations strongly altered miRNA expression patterns in tumors, which was functionally validated in cell lines expressing mutant *DROSHA*.

Significance

Very few driver genes have been identified thus far in Wilms tumors. Our identification of two prominent pathways—SIX1/2 and DROSHA/DGCR8—implicated in kidney development and miRNA biogenesis, respectively, and both involved primarily in blastemal type Wilms tumorigenesis, provides insight into the biology of these tumors. This is extended by our finding of additional mutations in other kidney developmental genes and a very high rate of *IGF2* imprinting deregulation. Furthermore, the strong negative impact of *TP53* mutations calls for thorough evaluation of such events. Altogether, our findings broaden the spectrum of human cancer genes and may open avenues for stratification and therapeutic leads for Wilms tumors.

INTRODUCTION

Wilms tumor affects 1 in 10,000 children. The Wilms tumor suppressor gene *WT1* was one of the first tumor suppressor genes to be cloned (Call et al., 1990; Gessler et al., 1990), but the genetic basis of these tumors remains heterogeneous and is still poorly understood (Huff, 2011). Only about one-third of tumors carry either a *WT1* mutation—often combined with a *CTNNB1* mutation—or an alteration affecting the *WTX* gene (Rivera et al., 2007; Ruteshouser et al., 2008; Wegert et al., 2009). *TP53* mutations appear to be restricted to rare anaplastic tumors (Bardeesy et al., 1994), and other changes (e.g., alterations in *MYCN*, *FBXW7*) are similarly uncommon (Williams et al., 2010), leaving a significant fraction of cases without an identified "driver" genetic defect. Characteristic chromosomal aberrations include deletions of chromosomes 1p and 16q as well as gain of chromosome 1q (15%–30% each), but the critical genes in these regions remain elusive (Grundy et al., 2005; Segers et al., 2013). There is a strong epigenetic contribution to tumorigenesis since more than one-third of cases exhibit loss of the maternal allele of chromosome 11p15, or loss of imprinting (LOI) in the *IGF2/H19* gene cluster (Scott et al., 2012). The limited prevalence and prognostic value of currently known genetic alterations in Wilms tumors indicate that significant drivers of initiation and progression remain to be discovered.

Patients are treated according to either Société International d'Oncologie Pédiatrique (SIOP) (Europe and other countries) or Children's Oncology Group (COG) (North America) protocols (Dome et al., 2013; Vujanić and Sandstedt, 2010). While COG protocols are based on primary surgery followed by chemotherapy, SIOP patients usually receive preoperative chemotherapy, followed by surgery and adjusted postoperative chemotherapy and radiotherapy. The difference in treatment protocols leads to important differences in histological presentation and prognostic classification (Weirich et al., 2001). Wilms tumors are histologically diverse, with variable contributions of blastemal, stromal, and epithelial elements. While 35% of primarily resected tumors are classified as blastemal predominant, this fraction drops to 9.5% for cases evaluated following preoperative chemotherapy (Weirich et al., 2001). Blastemal contribution per se is not of prognostic significance in primarily resected tumors. However, remaining viable blastema after preoperative chemotherapy (SIOP protocol) is clearly associated with adverse prognosis and reduced relapse-free survival (58.4% versus 86.7%) (Weirich et al., 2004). This is comparable to the adverse outcome seen in conjunction with diffuse anaplasia and associated *TP53* mutations (Lahoti et al., 1996). Therefore, characterization of the genetic basis of persistent blastema to identify corresponding biomarkers or effective therapeutic leads is of paramount clinical interest.

RESULTS

To define the genetic makeup of high-risk, blastemal type, postoperative chemotherapy Wilms tumors, we performed exome sequencing of 53 such tumors, supplemented with two relapse samples, and corresponding normal controls. Three regressive type tumors were included since they were followed by blastemal type relapses (WT002 and WT044) or generated a blastema-only xenograft (WT046) (Table S1). Exome analysis (coverage 107–361 times) of these 58 cases was complemented by low-coverage (1.2–3.9 times) whole-genome sequencing to assess copy-number changes. Transcriptome analysis was carried out by RNA sequencing (RNA-seq) (average of 4.3×10^7 reads) and on Affymetrix U133 Plus 2.0 arrays. Detailed sequencing statistics are given in Table S2.

As expected for childhood tumors, the mean number of mutations was low. On average, there were 14 (range of 0–75) somatic single-nucleotide variations and small indels within protein coding exons per tumor with an average of 6 (0–15) non-synonymous mutations, including missense, stop loss, stop gain, and splicing mutations. This is within the range seen for other pediatric tumors, with an average of 0.14 mutations per Mb of coding DNA (Figure S1) (Lawrence et al., 2013). 303 genes were found to be mutated at least once, but only 18 genes were affected twice or more (Figures 1A and 1B; for a complete listing see Table S3). Seven of these genes (*CRLF1*, *DCHS1*, *ABCA7*, *RYR2*, *TTN*, *U2AF2*, and *NIPBL*) were not analyzed further due to limited evidence for functional relevance (see footnote in Table S3).

Stereotypic *SIX1/2* Hotspot Mutations in Wilms Tumors

The most prevalent somatic hotspot mutation was an A→G transition in exon 1 of the *SIX1* transcription factor gene that leads to a glutamine-to-arginine mutation at position 177 in the homeodomain in 6 of 58 cases (10%). In two instances, the wild-type (WT) allele was lost, while the other four tumors carried heterozygous mutations. Screening of a larger cohort of unselected Wilms tumors by Sanger sequencing of genomic DNA (n = 188) or allele-specific PCR (n = 529) identified 17 cases with the Q177R mutation in *SIX1*, the majority being heterozygous (Table 1; for details see Table S4). Intriguingly, two other tumors carried the equivalent Q177R mutation in *SIX2*, a highly homologous gene known to act downstream of *SIX1* in embryonic kidney development. A survey of 405 additional cases by allele-specific PCR identified another four *SIX2* mutant tumors. In addition, we found one truncating mutation in *SALL1*, a gene activated by SIX proteins during metanephric development, indicating that the entire signaling pathway may be critically involved in Wilms tumorigenesis.

In 16 of 16 cases analyzed, the *SIX1/2* mutations were somatic. Sequencing of cDNA showed that wild-type and mutant alleles for *SIX1* (n = 10) and *SIX2* (n = 1) were expressed equally, suggestive of a dominant effect. Besides blastemal tumors, the mutations were also detected in regressive and necrotic tumors that are thought to be derived from chemotherapy-sensitive blastema, albeit at lower frequencies (Table 1). The much higher incidence of *SIX1/2* mutations in tumors with chemotherapy-resistant blastema (14.1% [blastemal] versus 3.4% [regressive/necrotic], and 0.7% [others] for *SIX1*) may indicate that these mutations confer enhanced resistance to currently used drugs.

SIX1 and SIX2 have been proposed as blastemal markers in Wilms tumors before, but no hint toward a function as a tumorigenic driver has been identified to date (Sehic et al., 2012; Senanayake et al., 2013). We detected strong nuclear staining for SIX1 and SIX2 in blastemal cells, while epithelial and stromal components remained almost completely negative. Importantly, there was no obvious difference between blastemal tumors with or without *SIX1* or *SIX2* mutations (Figure 2A).

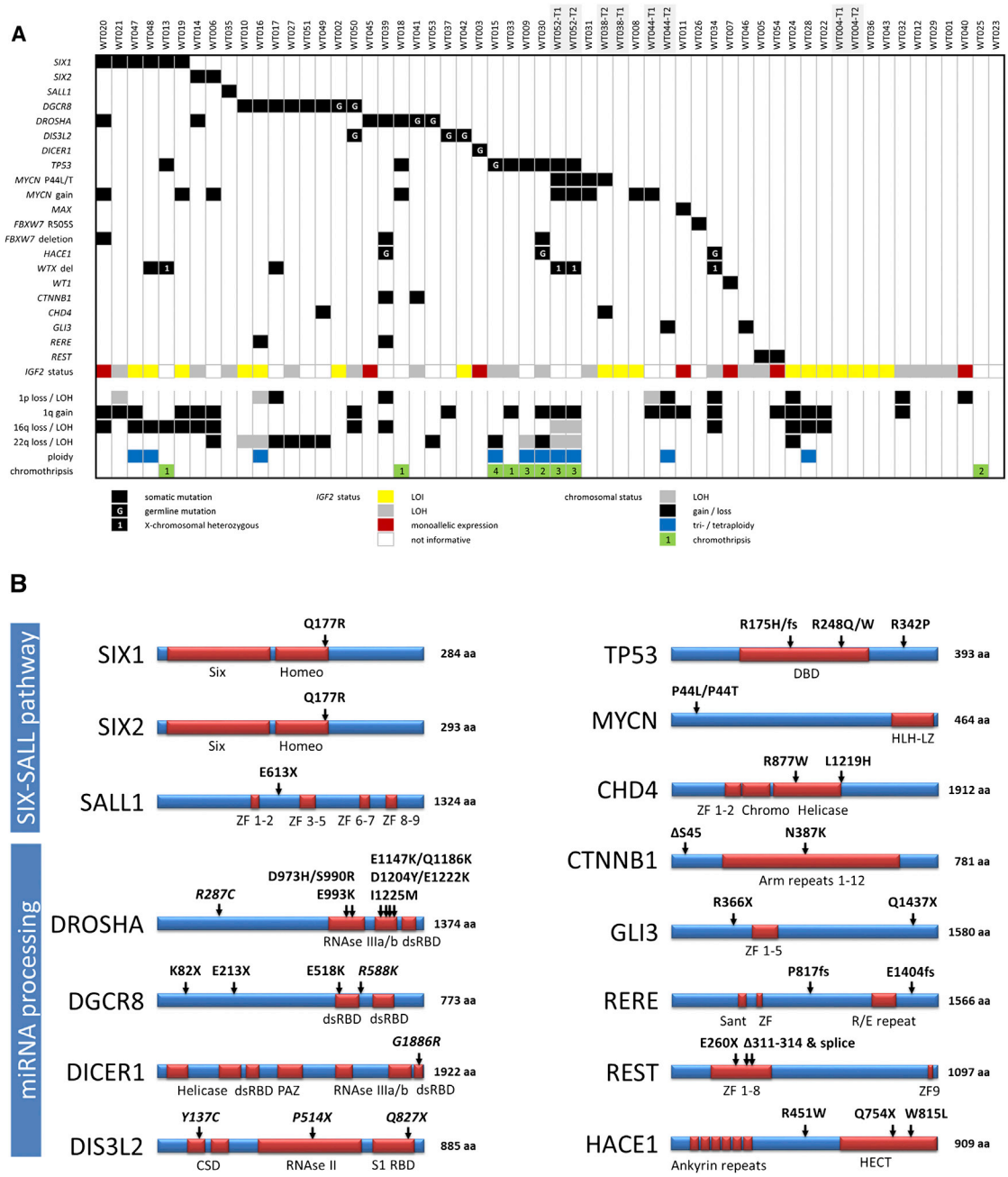

Figure 1. Mutation Analysis of Wilms Tumors

(A) Presence of somatic or germline (G) mutations is indicated by black boxes. For *WTX*, (1) specifies a hemizygous deletion in a female. The *IGF2* imprinting status is given as LOI, LOH, or regular monoallelic expression. In this case empty fields indicate missing or non-informative *IGF2* mRNA expression data and presence of two DNA alleles. The genomic aberrations at each of the frequently altered regions and triploidy/tetraploidy are color coded. For chromothripsis patterns the number of affected chromosomes is given.

(B) Recurrent somatic mutations in blastemal type Wilms tumors and selected single mutations affecting the same pathways. The location of coding and splice site mutations as well as known protein domains are highlighted. Germline variants are shown in italics.

See also Figure S1 and Tables S1, S2, and S3.

SIX1/2 Mutations Are Associated with a Proliferation and Kidney Progenitor Cell Signature

To characterize the molecular signature of *SIX1/2* mutations in vivo, we performed gene expression analysis of 62 tumors, including 32 with blastemal type histology, using Affymetrix arrays. Unsupervised cluster analysis separated the tumors into two prominent groups (Figure 2B). Group 1, enriched for blastemal type tumors (20/27) and characterized by upregulation of cell-cycle genes and genes involved in kidney development, contained all but two cases mutant for *SIX1/2* (Figure 2B). Both

Table 1. Mutation Frequency in Wilms Tumors According to Histological Subtype

	Histotype	Completely Necrotic	Epithelial Type	Stromal Type	Mixed Type	Regressive Type	Focal Anaplasia	Blastemal, before Chemotherapy	Blastemal Type	Diffuse Anaplasia	Nephroblastomatosis	Total
SIX1	Mutant	1/25	0/62	0/74	2/209	8/237	0/14	0/27	11/79	1/26	0/25	23/777
	Mutant (%)	4.0	0.0	0.0	1.0	3.4	0.0	0.0	14.1	3.8	0.0	3.0
SIX2	Mutant	1/25	0/64	0/76	1/75	1/77	0/6	0/26	3/75	0/27	0/12	6/463
	Mutant (%)	4.0	0.0	0.0	1.3	1.3	0.0	0.0	4.0	0.0	0.0	1.3
DROSHA	Mutant	1/25	0/64	1/76	1/101	7/102	2/9	3/26	7/77	3/27	0/18	25/525
	Mutant (%)	4.0	0.0	1.3	1.0	6.9	22.2	11.5	9.1	11.1	0.0	4.8
DGCR8	Mutant	0/26	0/62	0/74	8/213	10/235	0/14	0/26	7/77	1/27	0/23	26/777
	Mutant (%)	0.0	0.0	0.0	3.8	0.0	0.0	0.0	9.1	3.7	0.0	3.3
MYCN	Mutant	0/6	0/11	1/17	0/73	3/69	0/6	0/6	4/60	0/12	0/10	8/270
	Mutant (%)	0.0	0.0	5.9	0.0	4.3	0.0	0.0	6.7	0.0	0.0	3.0

See also Table S4.

SIX1/2 mutants in group 2, however, did not express *SIX1* or *SIX2*. All tumors in group 1 expressed high levels of *SIX1/2*, while expression levels in group 2 tumors were generally lower (Figures 2C and 2D). Interestingly, the eight *SIX1/2* mutants in group 1 all clustered together. A direct comparison of these *SIX1/2* mutants with the other 19 tumors in group 1 (all wild-type for *SIX1/2*) showed that many cell-cycle genes, already upregulated in group 1 tumors, are even further upregulated in *SIX1/2* mutant tumors (Figures 2E–2H). Group 1 tumors are further characterized by a concerted and strong expression of other *SIX* and *SALL* family members and the *SIX* cofactor gene *EYA1*, together with other kidney developmental genes (e.g., *CITED1*, *NCAM1*, *GDNF*, *REST*, and *MYCN*), indicative of a kidney progenitor cell state. Group 2 tumors are far more heterogeneous, with a stronger expression of genes involved in differentiation and maturation (transport, adhesion, extracellular matrix secretion) or inflammatory/immune responses and a less prominent association with specific mutations (Figure 2B).

SIX1 Mutations Alter DNA Binding

The known crystal structure of the SIX1 protein suggests that the Q177R mutation affects its DNA binding properties since superposition of the structurally highly conserved homeodomain fold onto the ternary complex formed between HoxB1-Pbx1 and DNA (Piper et al., 1999) places this residue in the major groove of the bound DNA (Figure 3A) (Patrick et al., 2013). Activation of the promoters of the well-established SIX1/2 targets *SIX2* and *SALL1* is not altered in luciferase assays, however, and wild-type and mutant SIX1 locates to the nucleus (Figures 2A, 3B, and S2).

To search for in vivo differences in DNA binding, we performed chromatin immunoprecipitation sequencing (ChIP-seq) using an SIX1 antibody. Two tumors with high levels of *SIX1* WT mRNA (WT010/WT088) and one tumor with comparable expression of a homozygous SIX1-Q177R mutation (WT047) were used; ~60,000 peaks were identified in each case. Binding motif analysis extracted a consensus SIX1 motif in the two cases with WT SIX1 (correlation of 0.98 and 0.95), while the mutant tumor only yielded a more divergent motif (correlation of 0.86) (Figure 3C; Table S5). Intriguingly, peaks with significantly reduced binding in the mutant tumor, where WT SIX1 is presumed to bind more strongly, still allowed retrieval of an SIX1 consensus site (correlation of 0.93). However, peaks with increased binding in the mutant tumor generated an even more divergent motif (correlation of 0.69), pointing to a distinct, SIX1-Q177R preferred site. Key differences are the loss of a requirement for TG at positions 7 and 8 and the gain of a C requirement at position 10 in the binding motif.

These data suggest that the Q177R mutation shifts DNA binding specificity, which may induce subtle changes in the gene regulatory capacity of SIX1, in line with the gene expression analysis in group 1 tumors described above. An example is the upregulation of *TGFA* in *SIX1* mutant tumors and the enhanced binding of SIX1-Q177R immediately upstream of the transcription start site and in two intronic regions, harboring sequences corresponding to the mutant-specific motif (Figures 3D and 3E). Full elucidation of the functional impact of *SIX1* mutations will require analysis of a larger set of tumors to derive final conclusions.

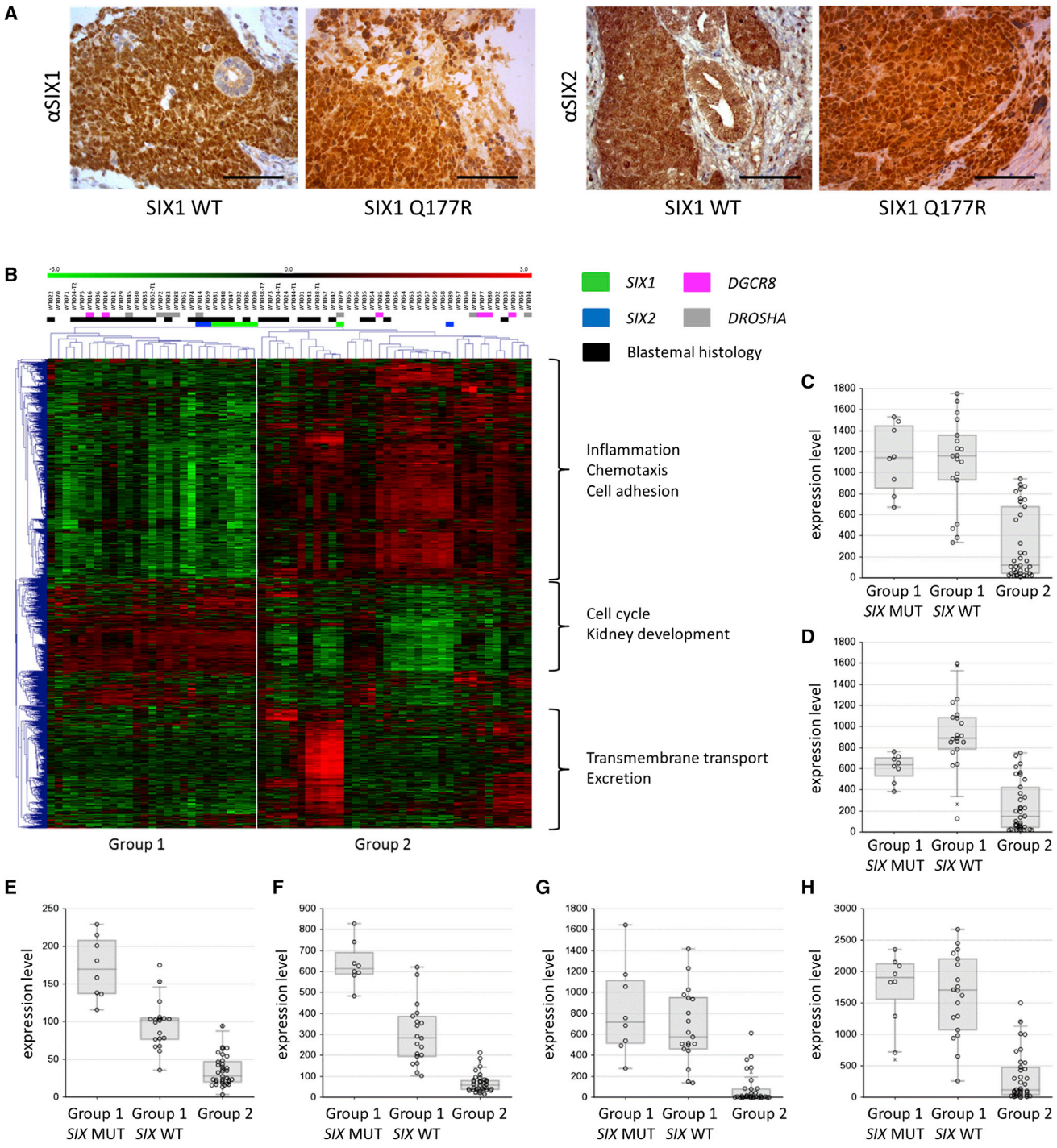

Figure 2. Expression Analysis in *SIX* Mutant Wilms Tumors

(A) Examples of immunohistochemical staining with SIX1 and SIX2 antisera in *SIX1* WT and mutant (Q177R) tumors. Note that blastemal nuclei show prominent staining whereas the epithelial component (tubulus) has no nuclear expression, only a weak cytoplasmic positivity. Scale bar, 50 μm.

(B) Gene expression profiling of 62 Wilms tumors. 35 cases are from the exome analysis cohort, supplemented with tumors representing other histological subtypes. Mutations and blastemal subtype are indicated by colored boxes. Two main groups are identified upon K-means clustering that differ in expression of three gene classes as categorized by gene ontology (GO) term analysis.

(C–H) Expression profiles for *SIX1* (C), *SIX2* (D), *AURKB* (E), *BUB1B* (F), *CITED* (G), and *MYCN* (H) shown as boxplots with arbitrary expression units. Boxes represent the middle 50% of data (circles) with a central line at the median. Whiskers represent extremes (up to 1.5-fold box size).

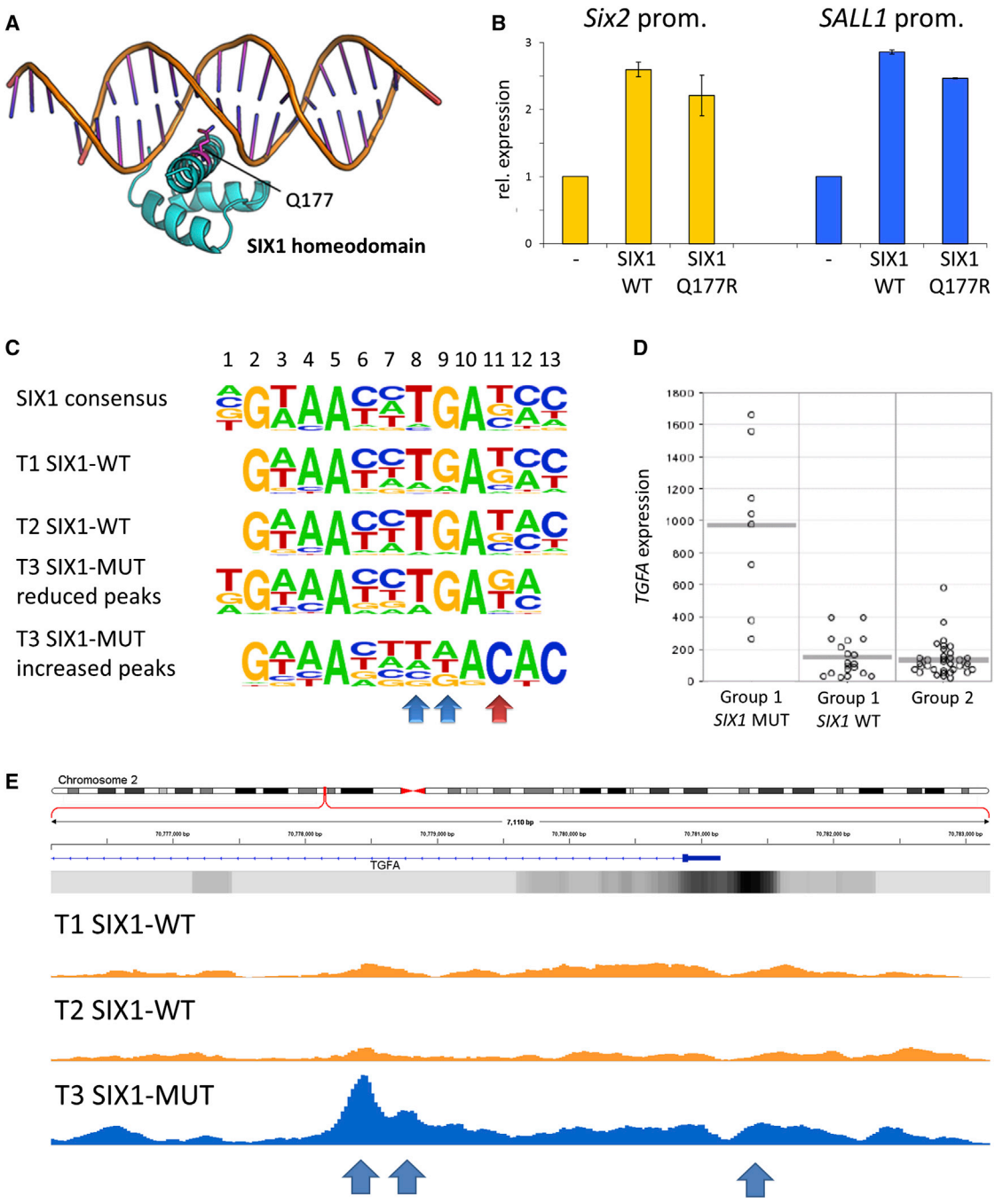

Figure 3. Functional Characterization of SIX1 Mutations

(A) Illustration of the Q177 containing helix of the SIX1 homeodomain inserted into the major groove of DNA. The high-resolution SIX1-EYA2 structure (PDB entry 4EGC) was superposed onto the coordinates of the HoxB1 crystal structure within its ternary complex with Pbx1 and DNA (PDB entry 1B72).

(B) Activation of the mouse *Six2* and the human *SALL1* promoters by expression of SIX1 or SIX1-Q177R in the murine mesonephric cell line M15. Values represent mean ± SD of luciferase expression levels relative to empty vector control (set to 1). Measurements were done in triplicates.

(C) SIX1 binding motifs identified in *SIX1* WT (T1, T2) and mutant (T3) tumors by ChIP-seq. Note that peaks reduced or increased in the SIX1 mutant tumor identify different binding motifs.

(D) Expression of *TGFA* in indicated group of tumors. Gray bar indicates mean expression value (arbitrary units).

(E) ChIP-seq profile around the *TGFA* start site. Three prominent peaks in tumor T3 harbor the variant SIX1 binding motif (arrows).

See also Table S5.

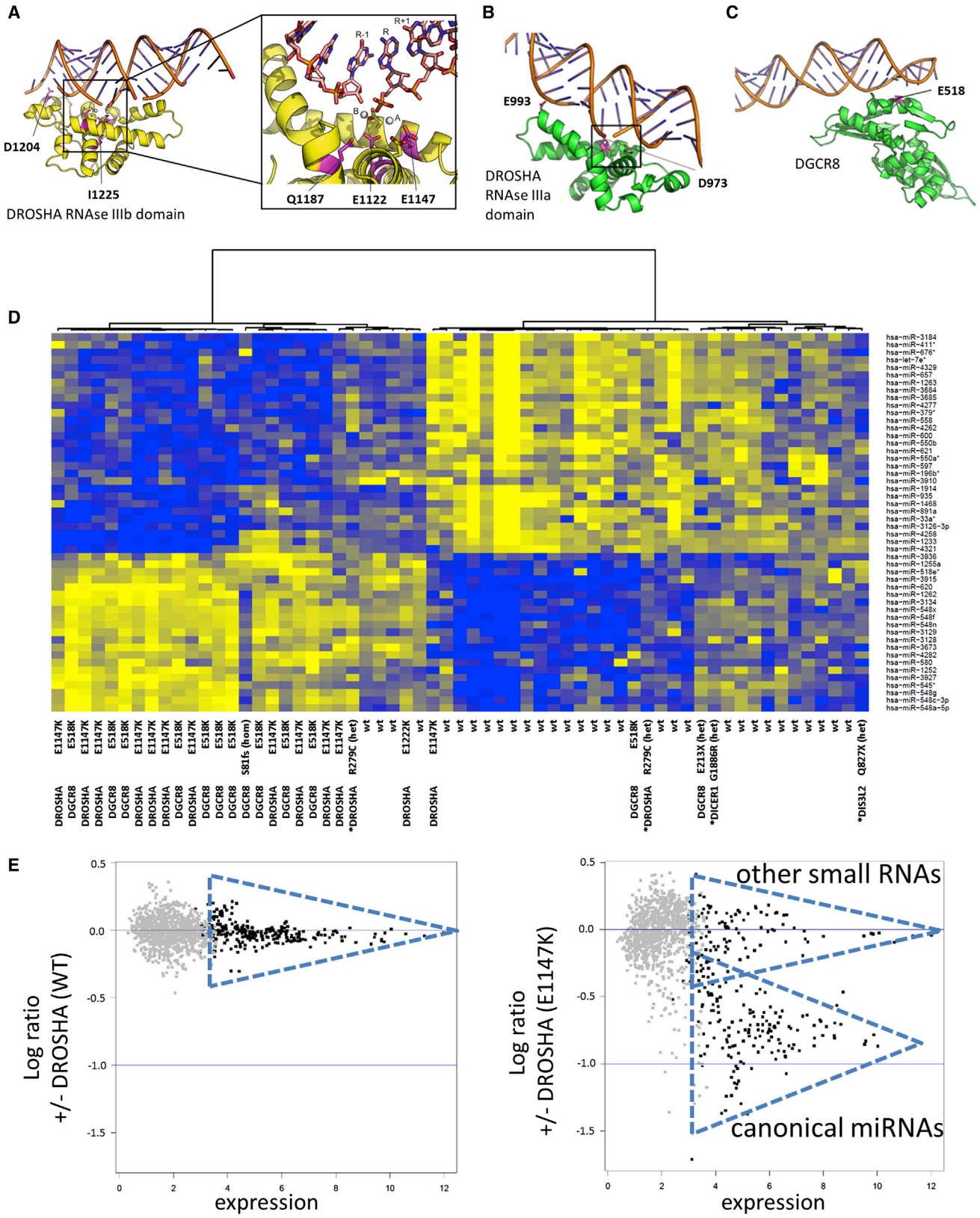

Figure 4. miRNA Processing Mutations and Their Functional Consequences

(A) Position of the DROSHA RNase IIIb domain mutations. The E1147K, Q1187K, and E1222K mutations affect the active site of the RNase IIIb domain and its two metal binding sites A and B, while I1225M disturbs an adjacent hydrophobic core. D1204Y involves a possible contact to the dsRNA substrate.

(legend continued on next page)

Microprocessor Gene Mutations in Wilms Tumors

The second most prevalent set of somatic mutations affected *DROSHA* and *DGCR8*, encoding the main components of the miRNA microprocessor complex (Figure 1). This complex processes primary miRNAs in the nucleus to form pre-miRNAs, which in turn are substrates to subsequent processing by DICER1 in the cytosol. Four of the five *DROSHA* mutations affect one of three key metal binding amino acids of the RNase IIIb domain that are thought to be essential for catalysis (Gan et al., 2006) (Figure 4A). In each case glutamic acid is replaced by lysine at amino acid 1147 (three times) or 1222 (once). The fifth mutation D973H is located in the catalytic center of the RNase IIIa domain (Gan et al., 2006) (Figure 4B).

Screening of another 363 cases by allele-specific PCR identified 13 additional tumors with the DROSHA E1147K mutation (Tables 1 and S4). Direct sequencing of the *DROSHA* cDNA for the RNase IIIa and IIIb domains in an independent set of 100 Wilms tumors detected seven additional somatic mutations (S990R, two times E993K, E1147K, Q1186K, D1204Y, and I1225M). The Q1186 and I1225 residues are again part of the catalytic center, while S990, E993, and D1204 are located outside. From a superposition of homology models of both DROSHA RNAase III domains with the high-resolution crystal structure of *Aquifex aeolicus* RNase III complexed with a double-stranded RNA (dsRNA) substrate (Gan et al., 2008), we predict that the D1204Y and E993K mutations are oriented toward and likely contact the dsRNA substrate (Figures 4A and 4B). Of note, these mutations were always heterozygous in tumor DNA and cDNA without evidence for additional alterations on the second allele. For eight tumors, multiple biopsies (up to six) were available, and all exhibited heterozygous mutations. This clearly is suggestive of a dominant effect.

The changes in the DROSHA partner protein DGCR8 were even more striking. Four tumors in the exome sequencing cohort showed hotspot mutations leading to a single amino acid alteration with charge reversal (E518K) in the RNA binding domain (Figure 4C). In one tumor, a homozygous single-nucleotide insertion resulted in a frameshift with early protein truncation after amino acid 81, while a sixth tumor had a heterozygous E213X nonsense mutation. Allele-specific PCR for the E518K alteration followed by sequencing on 719 additional cases revealed the presence of the identical mutation in 20 additional tumors, leading to a cumulative incidence of 3.2% (Tables 1 and S4).

In contrast to the heterozygous alterations in *DROSHA*, mutations in *DGCR8* were homozygous in many cases (Table S4). However, several tumors with missense mutations that retained a wild-type allele expressed only the mutant allele, indicating that the mutation must act recessive. *DGCR8* is located on chromosome 22q11 and the known adverse effect of loss of heterozygosity (LOH) of 22q (Klamt et al., 1998) may in part be due to the involvement of *DGCR8.* Indeed, of the six *DGCR8* mutant cases from the exome sequencing cohort, three had deletions and two had LOH of chromosome 22q.

Surprisingly, there was a striking sex bias in *DGCR8* mutations since 23 of 26 cases (88%; $p = 0.003$, χ^2 test) arose in girls, while there was a similar distribution of male and female patients in the entire cohort (343 versus 430) and for all other recurrent mutations. There is no evidence for sex-specific expression or imprinting in the corresponding genomic region and RNA sequencing data from non-mutant cases of our cohort did not provide evidence for monoallelic expression of other informative *DGCR8* SNPs that would explain this bias.

The known crystal structure of DGCR8 suggests that the amino acid change seen in Wilms tumors may disrupt the strong interaction of three neighboring amino acids via a hydrogen-bonding network (not shown). Although there is no co-structure available with bound RNA, superposition onto the ADAR2 double-stranded RNA binding motif (dsRBM)-RNA complex (Stefl et al., 2010) suggests that the mutated residue may be involved in readout of the minor groove or in contacts to the ribose/phosphate backbone (Figure 4C). This could have severe consequences for target selectivity and activity of the microprocessor complex.

There was a significant overlap of *DROSHA* and *SIX1* mutations with 17 *DROSHA*, 17 *SIX1*, and 6 double mutant tumors ($p < 10^{-6}$). On the other hand, a combined mutation of *SIX1* and *DGCR8* was detected just once, suggesting that only the link between *SIX1* and *DROSHA* may be functionally significant and synergistic.

Germline Mutations

Wherever DNA from blood leukocytes or adjacent normal kidney was available, we also checked for possible germline mutations. There were eight cases affecting *DROSHA* (two times R279C), *DGCR8* (two times K588R), *DICER1* (G1886R), and *DIS3L2* (Y137C, P514X, and Q827X), and some are predicted to be deleterious (Table S4). Although all mutations are truncating or affect conserved residues, only the *DIS3L2* P514X mutation became homozygous in the tumor, supportive of functional importance. These constitutional heterozygous mutations appear compatible with normal development, but may still pose an increased tumor risk as proposed by Foulkes et al. (2014) in the case of *DICER1*. Some of these mutations are also present at low frequency in reference exome sequences (Exome Aggregation Consortium

(B) The D973H mutation affects the active site of the DROSHA RNase IIIa domain (within the box) and its two metal binding sites, while E993K is located at a distant position involving a putative contact to the dsRNA substrate.

(C) The DGCR8 E518K mutation in a presumptive protein dsRNA complex modeled according to the known DGCR8 structure and a related ADAR2-dsRMB-RNA complex. Affected residues are rendered in magenta.

(D) miRNA expression profiling separates tumors with mutations in the microprocessor genes *DROSHA* and *DGCR8* from non-mutated controls. Hierarchical clustering was done with the 50 most discriminative small RNA features. miRNA processing mutations are listed with germline changes marked by asterisks. All probes had adj. p values of 1.1×10^{-6} or less.

(E) Changes of miRNA profiles in HEK293T cells upon inducible expression of wild-type or E1147K mutant DROSHA. Duplicates of biological replicas were hybridized onto Agilent miRNA arrays. RNAs with >50% presence calls by the feature extraction software are shown in black; all others are in gray. Triangles highlight clusters of small RNAs that either feature or lack characteristics of canonical miRNAs according to miRBase.

See also Table S6.

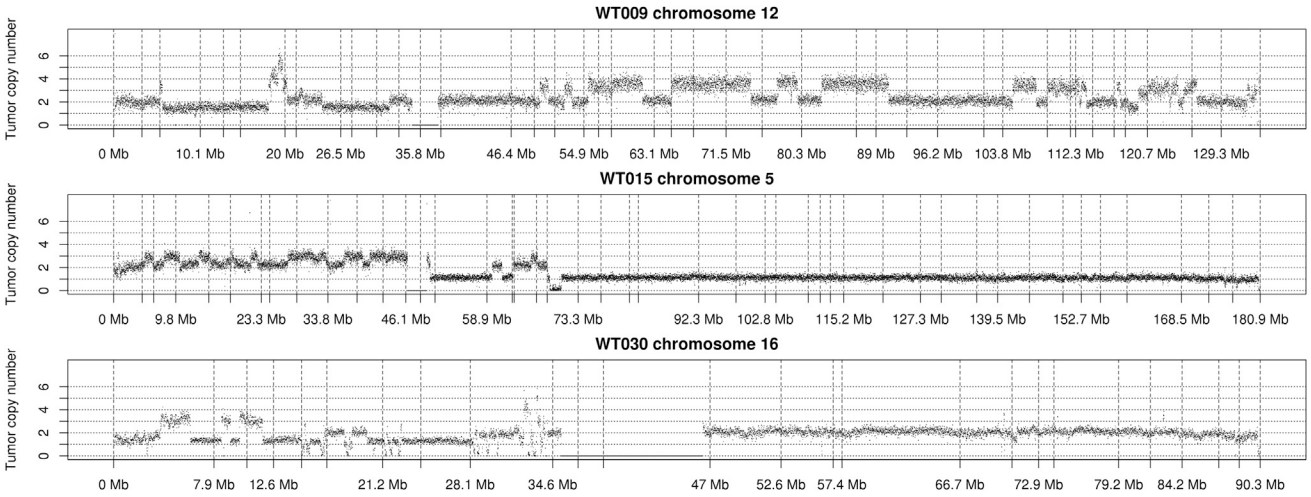

Figure 5. Examples of Chromothripsis Patterns in Wilms Tumors

Tumor and chromosome numbers are given above each graph that represents one affected chromosome each. Copy-number changes appear as deviation from the expected two copy values, calculated from the genome-wide median.

See also Figure S3 and Table S7.

[ExAC]; http://exac.broadinstitute.org/), but none of the more frequent *SIX1/2* or microprocessor mutations has been found there.

Microprocessor Mutations Alter miRNA Expression Patterns

DROSHA/DGCR8 mutations did not have a strong effect on gene expression levels as the mutant tumors did not cluster together like the *SIX1/2* mutants did (Figure 2B). We also characterized the effects of *DROSHA/DGCR8* mutations on miRNA processing and compared miRNA profiles in 30 *DROSHA/DGCR8/DICER1/DIS3L2* mutant with 31 non-mutant tumors. There was a clear distinction with *DROSHA/DGCR8* mutant tumors forming a separate group upon unsupervised hierarchical clustering based on the 50 most discriminative miRNAs (Figure 4D). Tumors with *DROSHA* and *DGCR8* mutations were intermingled upon clustering, suggesting that these mutations have very similar effects. Only two cases with common mutations had miRNA profiles indistinguishable from tumors devoid of microprocessor mutations. In total, 320 (27%) of small RNAs tested exhibited significant expression differences between wild-type and mutant tumors (adjusted [adj.] $p < 0.05$), indicative of broad alterations in miRNA processing (Table S6). Notably, the *DGCR8* stop mutations as well as the *DICER1*, *DIS3L2*, and N-terminal *DROSHA* mutations had limited or no effect on miRNA patterns, indicating that they may only affect a smaller subset of miRNAs.

To functionally assess *DROSHA* mutations, we generated human embryonic kidney 293T (HEK293T) cells with inducible overexpression of wild-type or mutant *DROSHA*. Expression levels of endogenous and transgene *DROSHA* mRNA were similar by qRT-PCR, mimicking the heterozygous mutations in Wilms tumors. Induction of WT DROSHA did not alter the miRNA pattern as tested on Agilent Technologies microarrays. Expression of the DROSHA E1147K mutant, however, led to a downregulation of many of the expressed small RNAs. All 145 miRNAs with significant regulation (adj. $p < 0.05$) showed a reduced expression (average fold-change of −1.7 times) upon DROSHA-E1147K induction (Figures 4E and 4F; Table S6). Strikingly, these RNAs are mostly classified as high-confidence miRNAs according to miRBase (Kozomara and Griffiths-Jones, 2014), while almost no short RNA with unaltered expression can be classified as canonical miRNA. This clearly is different from *DICER1* syndrome and points to a dominant and global miRNA processing defect of the *DROSHA* mutant in heterozygous tumor cells.

TP53 Mutations Are Associated with Aneuploidy, Chromothripsis, and Poor Outcome

The homozygous *TP53* mutations reported here affect known hotspots (R175, R248, and R342) or lead to a premature stop in six tumors, while a seventh tumor (WT030) has a homozygous deletion (Figures 1A and 1B; Table S3). Histology was classified as blastemal type, but some cases exhibited additional focal or even diffuse anaplasia. This is in line with the previous link of *TP53* mutations to anaplastic Wilms tumor and the presence of a histologic continuum including nuclear unrest (Bardeesy et al., 1994). These mutations seem to induce genomic instability since four of the tumors were tetraploid/aneuploid and all seven featured a chromothripsis pattern (Figures 1A, 5, and S3; Table S7). Of note, there was only a single case without *TP53* alteration that featured a chromothripsis pattern, further strengthening a causal link between germline or early somatic TP53 mutation and chromothripsis as proposed for medulloblastoma and several other entities (Rausch et al., 2012).

One of the *TP53* mutations (R342P; WT015) affecting the tetramerization domain was also present in the germline, indicative of Li-Fraumeni syndrome. Most importantly, all seven patients with *TP53* mutations died. There were only two additional fatal cases in our series without a *TP53* alteration, highlighting the massive negative impact of such mutations. Even with an additional 11 cases in our cohort showing active disease (1) or short follow-up of less than 2 years (10), it appears that

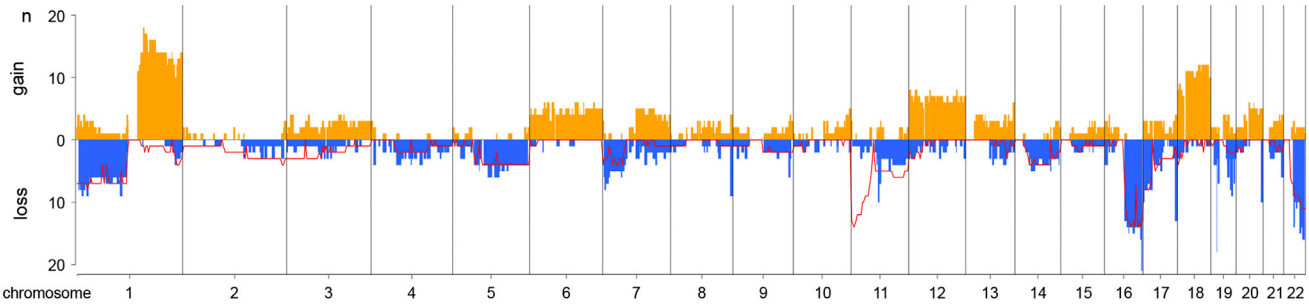

Figure 6. Chromosomal Copy-Number Changes and Allele Loss in Wilms Tumors

Copy-number changes were assessed on low-coverage whole-genome sequences, quantified using 10-kb bins and then mapped to cytobands. The red line denotes abundance of allele loss (LOH) based on BAF. See also Table S7.

TP53 mutations are the most relevant aberration mediating poor outcome.

Mutations Affecting *MYCN* in Wilms Tumors

The *MYCN* gene was affected in two ways: one tumor showed point mutations in both alleles of the *MYCN* gene (WT052: P44L, P44T) and the P44L mutation was also found in tumors WT031 and WT038—in the latter only in a fraction of cells (Figure 1A). Furthermore, low copy amplification of *MYCN* including only one to seven flanking genes was seen in five cases (including WT052), based on whole-genome and exome analyses, yielding a 14% frequency of *MYCN* alterations in blastemal type tumors. Analysis of another 200 Wilms tumors by multiplex ligation-dependent probe amplification (MLPA) yielded a similar incidence of 16.5% low-copy number *MYCN* gain with no apparent preference for certain histological subtypes. Allele-specific PCR revealed P44L mutations in three regressive and one stromal type tumors, indicating that these are recurrent events (Tables 1 and S4), with an overall frequency of *MYCN* alterations of 18.5%. There were also tumors with a missense mutation (subclonal in WT026) or focal heterozygous deletions of *FBXW7* (four times), which is known to destabilize MYCN (Figure 1A). Furthermore, one tumor had a somatic R60Q mutation in *MAX*, which encodes a MYC heterodimerization partner that is the most frequent change reported in the COSMIC database (https://www.sanger.ac.uk). The mutation strongly alters the main contact to the phosphate backbone of DNA and may shift the balance toward pro-tumorigenic MYCN/MIZ1 complexes. The effect of MYCN mutation status on expression levels could not be quantitated due to insufficient numbers of cases in the cohort analyzed. In general, expression of *MYCN* correlated with high *SIX1/2* expression and a proliferation signature (Figure 2H).

Additional Mutations Are Found at Lower Frequency

WTX alterations are less frequent in our cohort compared to unselected Wilms tumors (Wegert et al., 2009), with complete deletions in two males and hemizygous losses in three females (Figure 1A). In two female cases RNA was available, with one exhibiting very low *WTX* expression (<10% average), suggestive of a functional deletion. The well-established Wilms tumor genes *CTNNB1* and *WT1* were mutated twice and once, respectively. This low incidence is certainly due to their preferential association with a different, i.e., stromal subtype. There were three cases with germline mutations in *HACE1*, a gene implicated in Wilms tumor formation, but it is unclear whether the alterations seen in prior studies instead affect the neighboring *LIN28B* locus that is clearly involved in Wilms tumor formation (Slade et al., 2010; Urbach et al., 2014; Viswanathan et al., 2009).

Other mutations detected twice within the screening cohort (*CHD4*, *GLI3*, *REST*, and *RERE*) point toward an impaired differentiation of kidney precursor cells since these genes are known to be expressed conspicuously during kidney development or maintain key roles in precursor cell differentiation.

Imprinting Defects and Chromosomal Imbalances Are Frequent in Blastemal Type Wilms Tumors

There is a very high incidence of chromosome 11p15 alterations, predicted to affect *IGF2* expression in our series of blastemal type tumors. The *IGF2* gene is active on the paternal allele only, due to genomic imprinting. LOI or LOH involving 11p15 with almost invariant duplication of the paternal allele lead to two active gene copies. Only 8 of 42 informative cases had regular monoallelic expression, while 15 showed biallelic expression (LOI) and another 19 exhibited copy-number neutral LOH with likely two active paternal *IGF2* alleles (Figure 1A). Thus, 81% of cases show evidence of imprinting defects and allele loss with concomitant increased expression of *IGF2* (average increase: 2.4 times, LOI; 2.7 times, LOH). The adjacent *H19* gene shows monoallelic expression in all tumors, indicative of an uncoupling of *H19* and *IGF2* imprinting, which has been reported previously (Bjornsson et al., 2007). This clearly demonstrates that the *IGF2* status is of particular importance for blastemal type Wilms tumors.

The recurrent gene mutations reported here affect ~74% of tumor samples and substantially expand the known repertoire of driver genes in Wilms tumorigenesis. In addition, there are further recurrent genomic copy-number alterations (CNAs) and allelic losses that affect multiple chromosomes or segments thereof in >75% of tumors (Figures 1A and 6; Table S7). The most frequent change is gain of chromosome 1q, often in conjunction with deletion of 16q, suggestive of an unbalanced t(1q:16q) translocation or isochromosome 1q described cytogenetically previously (Segers et al., 2013). Deletions of chromosome 1p and 22q (location of *DGCR8*) are also frequent as are

gains of chromosomes 6, 7q, 12, or 18 (Table S7). These data are in general agreement with previous findings (Natrajan et al., 2006), but do not identify novel blastema-specific alterations.

DISCUSSION

Whole-genome analyses have provided insight into a number of tumor entities and have helped to expand the known repertoire of oncogenic driver mutations in human tumors (Lawrence et al., 2013). In pediatric Wilms tumors, only three genes (*WT1*, *CTNNB1*, and *WTX*) have been found mutated at $\geq$10% frequencies to date. In many cases, a clear-cut genetic defect is still missing. We now identify several additional genes that are candidate oncogenic drivers in Wilms tumors, and most of these genes are apparently specific for this tumor entity, suggesting a unique pathway of tumor formation.

The most striking additions to the repertoire of Wilms tumor genes are *SIX1*, *SIX2*, and the microprocessor components *DROSHA* and *DGCR8*. SIX1, SIX2, and SALL1 are key transcription factors for mouse kidney development and may characterize Wilms tumor initiating cells (Brodbeck and Englert, 2004; Pode-Shakked et al., 2013). They are essential for signaling and expansion of the blastemal cell compartment that is induced by the ureteric bud to proliferate and to differentiate into nephrons. Loss of any of these genes leads to kidney agenesis or reduced size, most likely due to reduced proliferation and premature differentiation of blastemal cells (Yu et al., 2004). In addition, *Six1* and *Six2* are part of a gene set that allows reprogramming of adult kidney tubule cells into nephron progenitors (Hendry et al., 2013). These observations imply that hyperactivation of this pathway may lead to excessive proliferation of blastemal cells and thus blastemal type Wilms tumors. Indeed, high expression of SIX1 and SIX2 has been reported in Wilms tumors (Sehic et al., 2012; Senanayake et al., 2013), but it remained unclear whether this represented an oncogenic driver or only reflected the blastemal differentiation state of tumor cells.

The somatic *SIX1* and *SIX2* mutations described here have not been reported before. However, a parallel study by Walz et al. (2015 in this issue of *Cancer Cell*) detected such mutations at a 7% frequency in a large cohort of favorable histology Wilms tumors, also with a preference for blastemal histology, thus validating our findings. The stereotypic location affecting a single amino acid residue that appears to be involved in DNA binding clearly points to a regulatory role. The heterozygous mutations and equal expression of both alleles in most cases suggests that novel functions are gained in a dominant manner. While mutant SIX1 can still activate classic target promoters, our ChIP-seq experiments uncovered a shift in DNA binding preference that is paralleled by discrete changes in expression profiles in mutant tumor samples. Thus, *SIX1/2* mutations may drive oncogenesis through subtle quantitative effects on a proliferation mRNA signature of embryonic precursor cells.

Germline mutations in *SIX1* were previously described in branchiootorenal (BOR) syndrome, but the *SIX1* mutations found in those patients are different from the somatic mutations described here and they only affect regions N terminal to Q177 (Ruf et al., 2004). Although BOR syndrome can be accompanied by renal developmental defects, there is no report of tumor predisposition, suggesting that the mechanisms are different. The *SALL1* mutation detected in one of our cases is similar to truncating mutations seen in Townes-Brocks syndrome, where rare kidney defects but no Wilms tumors were reported previously (Kohlhase et al., 1998).

The combined evidence from human tumor data and mouse knockout models thus supports a critical role for the SIX1/2 pathway not only in the control of kidney development but also as an oncogenic driver in malignant transformation that may be testable in animal models.

Processing defects of miRNAs have been implicated in several human tumors—including Wilms tumor—through *DICER1* mutations affecting the RNase IIIb domain (Wu et al., 2013). This leads to preferential processing of 3p versus 5p miRNAs (Anglesio et al., 2013). Although most of the *DROSHA* mutations in Wilms tumors map to the RNase IIIb domain, there is no evidence for such an effect. Our data rather suggest that the mutations lead to a global reduction in many miRNAs irrespective of their derivation from the 5′- or 3′-strand. Thus, these microprocessor mutations must act different from the ones observed in *DICER1* syndrome, which may be explained by the fact that incompletely processed pre-miRNAs will fail to be exported from the nucleus. For *DGCR8* there are no comparable alterations in the literature. While the highly specific E518K mutations in *DGCR8* point to a more focused processing defect, the similarity of miRNA profiles with *DROSHA* mutant tumors would argue instead for a global processing defect.

Mutations of the *let-7* miRNA processing factors *DIS3L2* (Perlman syndrome, predisposing to Wilms tumor) (Astuti et al., 2012) and *LIN28B* (tumor-specific translocations) (Viswanathan et al., 2009) already point to a critical role for miRNA processing in Wilms tumor. Furthermore, transgenic overexpression of *Lin28* in kidney precursors resulted in a mouse model of Wilms tumor formation (Urbach et al., 2014). The apparent limitation to *let-7* miRNAs reflects a clear difference to the microprocessor mutations with much broader specificity, which is also supported by the more regular miRNA patterns observed in our *DICER1* and *DIS3L2* mutant cases.

Similar mutations of *DROSHA* and *DGCR8*, as well as a small number of mutations in *XPO5* and *TARBP2* of unclear significance, have recently been reported together with altered miRNA patterns in mutant tumors (Rakheja et al., 2014; Torrezan et al., 2014; Walz et al., 2015). The large-scale study by Walz et al. (2015) furthermore identified a strong preference for blastemal histology, a high frequency of perilobar nephrogenic rests and imprinting defects, and a strong bias toward females in the case of *DGCR8* mutations. These studies likewise found heterozygous, dominant-negative *DROSHA* mutations, but homozygous *DGCR8* inactivation. Taken together with our results and the fact that *Dgcr8*$^{-/-}$ embryonic stem cells (ESCs) are unable to downregulate the self-renewal program and to proceed into differentiation (Melton et al., 2010), microprocessor genes appear to represent excellent candidates for drivers of blastemal type Wilms tumors. These mutations may facilitate evasion from the final round of precursor cell differentiation in the developing kidney, leading to continuous proliferation of blastemal precursor cells.

Although low-level *MYCN* amplification has been found in Wilms tumors before, the specific mutations of codon 44 within the Aurora A kinase interaction domain that regulates MYCN

stability has not. 14 *MYCN* alterations at codon 44 have been reported in the COSMIC database (endometrium, neural, intestine, and pancreas; https://www.sanger.ac.uk). Four cases of high-risk neuroblastoma showing this mutation have been published combined with evidence for a functional relevance from sequence homology with *MYC* and computational analyses (Pugh et al., 2013). Furthermore, *MYCN* amplification and overexpression have been associated with adverse prognosis in Wilms tumors (Williams et al., 2010; Zirn et al., 2006). This underscores the importance of the observed mutations and indicates that MYCN can be affected on multiple levels, especially since we detected further mutations of the *FXBW7* and *MAX* genes, which may also support oncogenic MYCN function.

An important outcome of the current profiling is that *TP53* mutations are a key contributor to lethality in blastemal type Wilms tumor. Such mutations have been described as being almost pathognomonic of anaplastic Wilms tumors. In our series, tumors with such mutations had anaplastic features to a varying extent and were invariably associated with chromothripsis and poor outcome. This indicates that screening for such alterations may be advisable in routine diagnosis, especially if there is any hint of anaplasia.

The overall low prevalence of gene mutations in blastemal type Wilms tumors clearly suggests that part of the molecular basis is yet to be uncovered, especially since most regions with recurrent chromosomal gains and losses lack clear candidate target genes. The very high incidence of *IGF2* alterations (LOI and LOH) with elevated mRNA expression in 81% of cases highlights that the known involvement of this gene in Wilms tumors seems to be even more important in blastemal type tumors, where IGF2 may serve as a growth and survival factor for blastemal cells.

Our identification of two prominent pathways—SIX1/2 and DROSHA/DGCR8—involved preferentially in blastemal type tumors provides insight into the biology of these tumors. Notably, these genes have not been found as mutated drivers in other tumor types before, suggesting that blastemal type Wilms tumors represent a very special molecular entity, even among pediatric cancer. Several of the genes mutated at lower frequency are involved in the control of progenitor cell self-renewal and the exit from proliferative compartments into terminal differentiation. This clearly suggests that in blastemal type Wilms tumors these progenitor cells fail to exit the physiologic embryonic growth compartment, which should make tumors amenable to differentiation-inducing therapies. A better definition of high-risk cases based on these candidate genes may in addition allow for further reduction in treatment intensity for subtypes that have an excellent prognosis with current regimens.

EXPERIMENTAL PROCEDURES

See Supplemental Experimental Procedures for details.

Samples

Wilms tumor and control tissues were obtained from the German SIOP93-01/GPOH and SIOP2001/GPOH studies and collaborating European centers. All subjects (or their parents) provided written consent for tumor banking and future research use according to national regulations: Ethikkommission der Ärztekammer des Saarlandes, 136/01 (Germany); Trent MREC/98/04/023/BD2 (the Netherlands); Ethics Committee Kanton Zurich (Switzerland) within an international clinical study (Nr 6/02); Trent MREC/01/4/086 (UK); Medical Research Ethics Committee of Our Lady's Children's Hospital, Crumlin, Dublin 12 (Ireland); and Regional Andalousian Ethics Committee, Seville (Spain). Sample names were coded at the sites of collection and further pseudonymized for central processing.

DNA Sequence Data Generation and Processing

Whole-genome sequencing libraries were prepared using Illumina v.2 protocols. Exome capturing was carried out with Agilent SureSelect Human All Exon v.4 50 Mb in-solution capture reagents. Paired-end DNA sequencing reads (Illumina HiSeq 2000) were mapped to the 1,000 genomes phase 2 reference assembly (hs37d5) using BWA and alignments were merged using SAMtools (Li et al., 2009). PCR duplicates were marked using Picards tools (http://broadinstitute.github.io/picard).

DNA Variant Detection

Single-nucleotide variants (SNVs) and small insertions/deletions (indels) were identified using an in-house analysis pipeline based on SAMtools, mpileup, and bcftools. CNAs were identified by use of low-coverage whole-genome sequencing reads of tumors and comparison of tumor and control exome pairs. LOH events were identified from B-allele frequency (BAF) plots generated from the SNV call using custom Perl scripts.

RNA-Seq Analysis

RNA-seq libraries were prepared using the Illumina TruSeq RNA Sample Preparation Kit v.2 and sequenced (Illumina HiSeq 2000) using 101-bp paired-end reads. RNA-seq reads were trimmed to remove low-quality bases and adaptor contamination using TrimGalore and mapped to the hs37d5 genome assembly with the GENCODE v.13 annotation as a transcript guide using Tophat. Expression values were reported as fragments per kilobase of exon per million fragments mapped (FPKM) as calculated by CuffDiff. Allele specific expression was calculated as an average of all DNA SNV positions with at least ten reads and minor allele frequency of 15%.

Verification of SNVs and Indels

For recurrently mutated genes, SNVs were verified by Sanger sequencing of genomic DNA. Expression of mutant alleles was tested on corresponding cDNA fragments. To screen larger tumor sets for distinct mutations, allele-specific PCR was performed with primers designed using WebSNAPER (http://pga.mgh.harvard.edu/cgi-bin/snap3/websnaper3.cgi), and variants were verified by direct sequencing.

Microarray Analysis

Wilms tumor RNA was analyzed on Affymetrix GeneChip Human Genome U133 Plus 2.0 arrays. The MAS5.0 algorithm was used for normalization. Data were analyzed using R2 (R2.amc.nl) or TM4 software (Saeed et al., 2003).

miRNA expression profiles were obtained using the Human miRNA Microarray Kit (release 16.0) and Feature Extraction Software (Agilent). Data were analyzed using the R/bioconductor package (http://www.bioconductor.org). Differences in miRNA expression were identified using the limma package (Smyth, 2005).

ChIP-Seq Data Generation and Analysis

Chromatin was immunoprecipitated from tumors with comparable expression of wild-type or mutant SIX1 (anti-SIX1, HPA001893, Sigma) by Active Motif. Sequencing was performed on the HiSeq 2500 platform using the Rapid Run settings. 100-bp paired-end reads were mapped to the 1,000 genomes phase 2 reference assembly (hs37d5) using BWA-MEM, and alignments were merged using SAMtools.

Mutation Modeling

Molecular images were generated with the program PYMOL (Schrödinger). For details on crystal structures used, see Supplemental Experimental Procedures.

ACCESSION NUMBERS

Sequencing data are accessible at European Genome-phenome Archive (http://www.ebi.ac.uk/ega) under accession number EGAS00001000906. Gene expression data have been deposited in GEO (http://www.ncbi.nlm.nih.gov/geo) under accession numbers GSE53224 (mRNA) and GSE57370/GSE60081 (miRNA).

SUPPLEMENTAL INFORMATION

Supplemental Information includes Supplemental Experimental Procedures, three figures, and seven tables and can be found with this article online at http://dx.doi.org/10.1016/j.ccell.2015.01.002.

AUTHOR CONTRIBUTIONS

J.W. and R. Vardapour prepared all samples and performed validations and functional tests. N.I., Z.G., M.B., S.K., and R.E. performed the bioinformatics analyses and provided the necessary framework. C. Geörg, B.Z., and S.B. performed quality control and validation experiments. N.L., A.K., P.v.S., R. Volckmann, J.K., R. Versteeg, and E.M. performed microarray analyses and contributed bioinformatics expertise. C. Grimm performed protein modeling. N.N., R.D.W., T.C., K.P.-J., T.A., M.J.O., P.K.B., F.N., G.A.T., H.v.T., M.M.v.d.H.-E., C.V., I.L., and N.G. provided essential materials, clinical data, and evaluations. S.M.P., M.K., and M.G. conceived the study, supervised all experiments, and prepared the manuscript.

ACKNOWLEDGMENTS

We thank all patients and their families for participation in this study. Collection of these samples would not have been possible without the efforts of clinicians, pathologists, and study nurses in many local hospitals in several countries that participated in the SIOP 2001 trial, the collection framework of the Competence Network Pediatric Oncology and Hematology in Germany, and the national tumor bank of the Children's Cancer and Leukaemia Group in the UK. We acknowledge Dr. Jan de Kraker (deceased) for his dedication and contribution as chair of SIOP 93-01 and SIOP 2001 trials. We thank Ron Schwessinger for implementing the VarScan pipeline and Pavel Komardin for data upload. Cancer Research UK supported sample collection in the UK. We thank Elizabeth Perlman for sharing of unpublished data from the parallel American sequencing study. This study was supported by grants from the DFG (Ge539/12-1), the Wilhelm-Sander-Stiftung, and the BMBF Competence Network Paediatric Oncology and Haematology to M.G. and by DFG Me917/20-1 to E.M.. We thank the DKFZ-Heidelberg Center for Personalized Oncology (DKFZ-HIPO) and the DKFZ sequencing core facility for technical support and funding through HIPO_H025.

Received: August 11, 2014
Revised: November 24, 2014
Accepted: January 9, 2015
Published: February 9, 2015

REFERENCES

Anglesio, M.S., Wang, Y., Yang, W., Senz, J., Wan, A., Heravi-Moussavi, A., Salamanca, C., Maines-Bandiera, S., Huntsman, D.G., and Morin, G.B. (2013). Cancer-associated somatic DICER1 hotspot mutations cause defective miRNA processing and reverse-strand expression bias to predominantly mature 3p strands through loss of 5p strand cleavage. J. Pathol. *229*, 400–409.

Astuti, D., Morris, M.R., Cooper, W.N., Staals, R.H., Wake, N.C., Fews, G.A., Gill, H., Gentle, D., Shuib, S., Ricketts, C.J., et al. (2012). Germline mutations in DIS3L2 cause the Perlman syndrome of overgrowth and Wilms tumor susceptibility. Nat. Genet. *44*, 277–284.

Bardeesy, N., Falkoff, D., Petruzzi, M.J., Nowak, N., Zabel, B., Adam, M., Aguiar, M.C., Grundy, P., Shows, T., and Pelletier, J. (1994). Anaplastic Wilms' tumour, a subtype displaying poor prognosis, harbours p53 gene mutations. Nat. Genet. *7*, 91–97.

Bjornsson, H.T., Brown, L.J., Fallin, M.D., Rongione, M.A., Bibikova, M., Wickham, E., Fan, J.B., and Feinberg, A.P. (2007). Epigenetic specificity of loss of imprinting of the IGF2 gene in Wilms tumors. J. Natl. Cancer Inst. *99*, 1270–1273.

Brodbeck, S., and Englert, C. (2004). Genetic determination of nephrogenesis: the Pax/Eya/Six gene network. Pediatr. Nephrol. *19*, 249–255.

Call, K.M., Glaser, T., Ito, C.Y., Buckler, A.J., Pelletier, J., Haber, D.A., Rose, E.A., Kral, A., Yeger, H., Lewis, W.H., et al. (1990). Isolation and characterization of a zinc finger polypeptide gene at the human chromosome 11 Wilms' tumor locus. Cell *60*, 509–520.

Dome, J.S., Fernandez, C.V., Mullen, E.A., Kalapurakal, J.A., Geller, J.I., Huff, V., Gratias, E.J., Dix, D.B., Ehrlich, P.F., Khanna, G., et al.; COG Renal Tumors Committee (2013). Children's Oncology Group's 2013 blueprint for research: renal tumors. Pediatr. Blood Cancer *60*, 994–1000.

Foulkes, W.D., Priest, J.R., and Duchaine, T.F. (2014). DICER1: mutations, microRNAs and mechanisms. Nat. Rev. Cancer *14*, 662–672.

Gan, J., Tropea, J.E., Austin, B.P., Court, D.L., Waugh, D.S., and Ji, X. (2006). Structural insight into the mechanism of double-stranded RNA processing by ribonuclease III. Cell *124*, 355–366.

Gan, J., Shaw, G., Tropea, J.E., Waugh, D.S., Court, D.L., and Ji, X. (2008). A stepwise model for double-stranded RNA processing by ribonuclease III. Mol. Microbiol. *67*, 143–154.

Gessler, M., Poustka, A., Cavenee, W., Neve, R.L., Orkin, S.H., and Bruns, G.A. (1990). Homozygous deletion in Wilms tumours of a zinc-finger gene identified by chromosome jumping. Nature *343*, 774–778.

Grundy, P.E., Breslow, N.E., Li, S., Perlman, E., Beckwith, J.B., Ritchey, M.L., Shamberger, R.C., Haase, G.M., D'Angio, G.J., Donaldson, M., et al.; National Wilms Tumor Study Group (2005). Loss of heterozygosity for chromosomes 1p and 16q is an adverse prognostic factor in favorable-histology Wilms tumor: a report from the National Wilms Tumor Study Group. J. Clin. Oncol. *23*, 7312–7321.

Hendry, C.E., Vanslambrouck, J.M., Ineson, J., Suhaimi, N., Takasato, M., Rae, F., and Little, M.H. (2013). Direct transcriptional reprogramming of adult cells to embryonic nephron progenitors. J. Am. Soc. Nephrol. *24*, 1424–1434.

Huff, V. (2011). Wilms' tumours: about tumour suppressor genes, an oncogene and a chameleon gene. Nat. Rev. Cancer *11*, 111–121.

Klamt, B., Schulze, M., Thäte, C., Mares, J., Goetz, P., Kodet, R., Scheulen, W., Weirich, A., Graf, N., and Gessler, M. (1998). Allele loss in Wilms tumors of chromosome arms 11q, 16q, and 22q correlate with clinicopathological parameters. Genes Chromosomes Cancer *22*, 287–294.

Kohlhase, J., Wischermann, A., Reichenbach, H., Froster, U., and Engel, W. (1998). Mutations in the SALL1 putative transcription factor gene cause Townes-Brocks syndrome. Nat. Genet. *18*, 81–83.

Kozomara, A., and Griffiths-Jones, S. (2014). miRBase: annotating high confidence microRNAs using deep sequencing data. Nucleic Acids Res. *42*, D68–D73.

Lahoti, C., Thorner, P., Malkin, D., and Yeger, H. (1996). Immunohistochemical detection of p53 in Wilms' tumors correlates with unfavorable outcome. Am. J. Pathol. *148*, 1577–1589.

Lawrence, M.S., Stojanov, P., Polak, P., Kryukov, G.V., Cibulskis, K., Sivachenko, A., Carter, S.L., Stewart, C., Mermel, C.H., Roberts, S.A., et al. (2013). Mutational heterogeneity in cancer and the search for new cancer-associated genes. Nature *499*, 214–218.

Li, H., Handsaker, B., Wysoker, A., Fennell, T., Ruan, J., Homer, N., Marth, G., Abecasis, G., and Durbin, R.; 1000 Genome Project Data Processing Subgroup (2009). The Sequence Alignment/Map format and SAMtools. Bioinformatics *25*, 2078–2079.

Melton, C., Judson, R.L., and Blelloch, R. (2010). Opposing microRNA families regulate self-renewal in mouse embryonic stem cells. Nature *463*, 621–626.

Natrajan, R., Williams, R.D., Hing, S.N., Mackay, A., Reis-Filho, J.S., Fenwick, K., Iravani, M., Valgeirsson, H., Grigoriadis, A., Langford, C.F., et al. (2006). Array CGH profiling of favourable histology Wilms tumours reveals novel gains and losses associated with relapse. J. Pathol. *210*, 49–58.

Patrick, A.N., Cabrera, J.H., Smith, A.L., Chen, X.S., Ford, H.L., and Zhao, R. (2013). Structure-function analyses of the human SIX1-EYA2 complex reveal insights into metastasis and BOR syndrome. Nat. Struct. Mol. Biol. *20*, 447–453.

Piper, D.E., Batchelor, A.H., Chang, C.P., Cleary, M.L., and Wolberger, C. (1999). Structure of a HoxB1-Pbx1 heterodimer bound to DNA: role of the hexapeptide and a fourth homeodomain helix in complex formation. Cell *96*, 587–597.

Pode-Shakked, N., Shukrun, R., Mark-Danieli, M., Tsvetkov, P., Bahar, S., Pri-Chen, S., Goldstein, R.S., Rom-Gross, E., Mor, Y., Fridman, E., et al. (2013). The isolation and characterization of renal cancer initiating cells from human Wilms' tumour xenografts unveils new therapeutic targets. EMBO Mol. Med. *5*, 18–37.

Pugh, T.J., Morozova, O., Attiyeh, E.F., Asgharzadeh, S., Wei, J.S., Auclair, D., Carter, S.L., Cibulskis, K., Hanna, M., Kiezun, A., et al. (2013). The genetic landscape of high-risk neuroblastoma. Nat. Genet. *45*, 279–284.

Rakheja, D., Chen, K.S., Liu, Y., Shukla, A.A., Schmid, V., Chang, T.C., Khokhar, S., Wickiser, J.E., Karandikar, N.J., Malter, J.S., et al. (2014). Somatic mutations in DROSHA and DICER1 impair microRNA biogenesis through distinct mechanisms in Wilms tumours. Nat. Commun. *2*, 4802.

Rausch, T., Jones, D.T., Zapatka, M., Stütz, A.M., Zichner, T., Weischenfeldt, J., Jäger, N., Remke, M., Shih, D., Northcott, P.A., et al. (2012). Genome sequencing of pediatric medulloblastoma links catastrophic DNA rearrangements with TP53 mutations. Cell *148*, 59–71.

Rivera, M.N., Kim, W.J., Wells, J., Driscoll, D.R., Brannigan, B.W., Han, M., Kim, J.C., Feinberg, A.P., Gerald, W.L., Vargas, S.O., et al. (2007). An X chromosome gene, WTX, is commonly inactivated in Wilms tumor. Science *315*, 642–645.

Ruf, R.G., Xu, P.X., Silvius, D., Otto, E.A., Beekmann, F., Muerb, U.T., Kumar, S., Neuhaus, T.J., Kemper, M.J., Raymond, R.M., Jr., et al. (2004). SIX1 mutations cause branchio-oto-renal syndrome by disruption of EYA1-SIX1-DNA complexes. Proc. Natl. Acad. Sci. USA *101*, 8090–8095.

Ruteshouser, E.C., Robinson, S.M., and Huff, V. (2008). Wilms tumor genetics: mutations in WT1, WTX, and CTNNB1 account for only about one-third of tumors. Genes Chromosomes Cancer *47*, 461–470.

Saeed, A.I., Sharov, V., White, J., Li, J., Liang, W., Bhagabati, N., Braisted, J., Klapa, M., Currier, T., Thiagarajan, M., et al. (2003). TM4: a free, open-source system for microarray data management and analysis. Biotechniques *34*, 374–378.

Scott, R.H., Murray, A., Baskcomb, L., Turnbull, C., Loveday, C., Al-Saadi, R., Williams, R., Breatnach, F., Gerrard, M., Hale, J., et al. (2012). Stratification of Wilms tumor by genetic and epigenetic analysis. Oncotarget *3*, 327–335.

Segers, H., van den Heuvel-Eibrink, M.M., Williams, R.D., van Tinteren, H., Vujanic, G., Pieters, R., Pritchard-Jones, K., and Bown, N.; Children's Cancer and Leukaemia Group and the UK Cancer Cytogenetics Group (2013). Gain of 1q is a marker of poor prognosis in Wilms' tumors. Genes Chromosomes Cancer *52*, 1065–1074.

Sehic, D., Karlsson, J., Sandstedt, B., and Gisselsson, D. (2012). SIX1 protein expression selectively identifies blastemal elements in Wilms tumor. Pediatr. Blood Cancer *59*, 62–68.

Senanayake, U., Koller, K., Pichler, M., Leuschner, I., Strohmaier, H., Hadler, U., Das, S., Hoefler, G., and Guertl, B. (2013). The pluripotent renal stem cell regulator SIX2 is activated in renal neoplasms and influences cellular proliferation and migration. Hum. Pathol. *44*, 336–345.

Slade, I., Stephens, P., Douglas, J., Barker, K., Stebbings, L., Abbaszadeh, F., Pritchard-Jones, K., Cole, R., Pizer, B., Stiller, C., et al.; FACT collaboration (2010). Constitutional translocation breakpoint mapping by genome-wide paired-end sequencing identifies HACE1 as a putative Wilms tumour susceptibility gene. J. Med. Genet. *47*, 342–347.

Smyth, G.K. (2005). limma: Linear Models for Microarray Data. In Bioinformatics and Computational Biology Solutions Using R and Bioconductor, R. Gentleman, V. Carey, W. Huber, R. Irizarry, and S. Dudoit, eds. (Springer), pp. 397–420.

Stefl, R., Oberstrass, F.C., Hood, J.L., Jourdan, M., Zimmermann, M., Skrisovska, L., Maris, C., Peng, L., Hofr, C., Emeson, R.B., and Allain, F.H. (2010). The solution structure of the ADAR2 dsRBM-RNA complex reveals a sequence-specific readout of the minor groove. Cell *143*, 225–237.

Torrezan, G.T., Ferreira, E.N., Nakahata, A.M., Barros, B.D., Castro, M.T., Correa, B.R., Krepischi, A.C., Olivieri, E.H., Cunha, I.W., Tabori, U., et al. (2014). Recurrent somatic mutation in DROSHA induces microRNA profile changes in Wilms tumour. Nat. Commun. *5*, 4039.

Urbach, A., Yermalovich, A., Zhang, J., Spina, C.S., Zhu, H., Perez-Atayde, A.R., Shukrun, R., Charlton, J., Sebire, N., Mifsud, W., et al. (2014). Lin28 sustains early renal progenitors and induces Wilms tumor. Genes Dev. *28*, 971–982.

Viswanathan, S.R., Powers, J.T., Einhorn, W., Hoshida, Y., Ng, T.L., Toffanin, S., O'Sullivan, M., Lu, J., Phillips, L.A., Lockhart, V.L., et al. (2009). Lin28 promotes transformation and is associated with advanced human malignancies. Nat. Genet. *41*, 843–848.

Vujanić, G.M., and Sandstedt, B. (2010). The pathology of Wilms' tumour (nephroblastoma): the International Society of Paediatric Oncology approach. J. Clin. Pathol. *63*, 102–109.

Walz, A.L., Ooms, A., Gadd, S., Gerhard, D.S., Smith, M.A., GuidryAuvil, J.M., Daoud Meerzaman, Chen, Q.-R., Hsu, C.H., Yan, C., et al. (2015). Recurrent DGCR8, DROSHA, and SIX homeodomain mutations in favorable histology Wilms tumors. Cancer Cell *27*, this issue, 286–297.

Wegert, J., Wittmann, S., Leuschner, I., Geissinger, E., Graf, N., and Gessler, M. (2009). WTX inactivation is a frequent, but late event in Wilms tumors without apparent clinical impact. Genes Chromosomes Cancer *48*, 1102–1111.

Weirich, A., Leuschner, I., Harms, D., Vujanic, G.M., Troger, J., Abel, U., Graf, N., Schmidt, D., Ludwig, R., and Voute, P.A. (2001). Clinical impact of histologic subtypes in localized non-anaplastic nephroblastoma treated according to the trial and study SIOP-9/GPOH. Ann. Oncol. *12*, 311–319.

Weirich, A., Ludwig, R., Graf, N., Abel, U., Leuschner, I., Vujanic, G.M., Mehls, O., Boos, J., Beck, J., Royer-Pokora, B., and Voute, P.A. (2004). Survival in nephroblastoma treated according to the trial and study SIOP-9/GPOH with respect to relapse and morbidity. Ann. Oncol. *15*, 808–820.

Williams, R.D., Al-Saadi, R., Chagtai, T., Popov, S., Messahel, B., Sebire, N., Gessler, M., Wegert, J., Graf, N., Leuschner, I., et al. (2010). Subtype-specific FBXW7 mutation and MYCN copy number gain in Wilms' tumor. Clin. Cancer Res. *16*, 2036–2045.

Wu, M.K., Sabbaghian, N., Xu, B., Addidou-Kalucki, S., Bernard, C., Zou, D., Reeve, A.E., Eccles, M.R., Cole, C., Choong, C.S., et al. (2013). Biallelic DICER1 mutations occur in Wilms tumours. J. Pathol. *230*, 154–164.

Yu, J., McMahon, A.P., and Valerius, M.T. (2004). Recent genetic studies of mouse kidney development. Curr. Opin. Genet. Dev. *14*, 550–557.

Zirn, B., Hartmann, O., Samans, B., Krause, M., Wittmann, S., Mertens, F., Graf, N., Eilers, M., and Gessler, M. (2006). Expression profiling of Wilms tumors reveals new candidate genes for different clinical parameters. Int. J. Cancer *118*, 1954–1962.